Materials Science-Poland, 30(4), 2012, pp. 382-389
http://www.materialsscience.pwr.wroc.pl/
DOI: 10.2478/s13536-012-0048-6

VERSITA

Synthesizing cysteine-coated magnetite nanoparticles as MRI contrast agent: Effect of pH and cysteine addition on particles size distribution

R. AHMADI[1]*, E. RANJBARNODEH[2] AND N. GU[3]

[1]1Research Center for Molecular and Cellular Imaging, Tehran University of Medical Sciences, Tehran, Iran
[2]Young Researchers Club, East Tehran Branch, Islamic Azad University, Tehran, Iran
[3]Jiangsu Key Laboratory of Biomaterials and Devices, Nanjing, China

Cysteine capped magnetite nanoparticles (10 to 20 nm) were synthesized via coprecipitation method under ultrasonic irradiation. The influence of pH value of the solution and cysteine addition on the size distribution and hydrodynamic size of nanoparticles were studied via TEM and PCS methods, respectively. The crystal structure and magnetic properties of the nanoparticles were characterized by XRD and VSM techniques, respectively. Coating density was calculated using TGA and TEM results. Cytotoxicity assessment performed by incubation of L929 cells, confirmed that ferrofluids are biocompatible. MRI studies conducted on rats demonstrated suitability of synthesized nanoparticles as contrast agents, especially for imaging of the lymph nodes.

Keywords: *coprecipitation, nanoparticles, electron microscopy, biocompatibility*

1. Introduction

Magnetite nanoparticles have been used in biological applications extensively such as drug delivery, Magnetic Resonance Imaging (MRI) contrast agent and cancer therapy [1–5]. Among different methods of magnetite nanoparticles synthesizing, such as coprecipitation [6, 7], sol-gel [8], hydrothermal [9] and thermal decomposition [10], the coprecipitation method has been used frequently due to its advantages. Magnetite nanoparticles tend to agglomerate during coprecipitation synthesizing due to their high specific surface area, surface energy and magnetization. In order to improve the size distribution and morphology of nanoparticles with small degree of agglomeration, coating of the magnetite nanoparticles with a capping agent is necessary. Up to now, amino acids have been used as biocompatible capping agents to control size distribution and prevent the agglomeration of various nanoparticles [11, 12]. Among all the amino acids, cysteine with three functional groups (Fig. 1) has a certain binding affinity to the iron atoms, which may control the size and the morphology of magnetite nanoparticles without any agglomeration. On the other hand, surface modification with small-molecule surfactants such as cysteine instead of conventional long-chain ones, such as dextran [13] and PEG [14], will result in an increase in the saturation magnetization due to the decrease in the amount of non-magnetic phase in the final product. However, ferrofluid stabilization in the case of cysteine is not as efficient as in case of long-chain surfactants and particles aggregation may occur. Using ultrasonic irradiation can decrease particles aggregation to some extent. Besides, ultrasonic-assisted synthesis of magnetite nanoparticles restricts growth of the crystal core due to ultrasonic cavitation mechanism [15].

Superparamagnetic iron oxide nanoparticles (USPIO) can be used as the MRI contrast agent for lymphatic system evaluation [16–19]. Iron oxide nanoparticles can create magnetic fields around themselves while being exposed to an external magnetic field due to their superparamagnetic

*E-mail: reahmady@yahoo.com

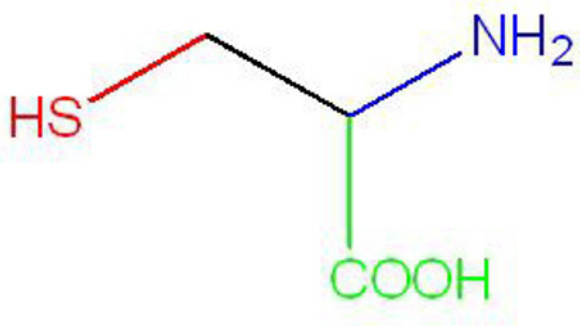

Fig. 1. Structure of cysteine.

properties; hence, the image signal intensity decreases at particles' accumulation regions as a result of rapid dephasing of the spins through a so-called susceptibility effect [16, 19]. So, images contrast improves due to enhancement of signal intensity difference between target tissues and the other ones. According to above-mentioned advantages of using cysteine, this amino acid was used as ferrofluid stabilizer in the present work. This surfactant has not been employed as biocapping agent for synthesizing MRI contrast agent yet, but has been used in similar biological applications [15, 20], confirming the biocompatibility of cysteine as a biocapping agent.

2. Experimental Procedure

2.1. Sample preparation

All the chemical reagents used in this research were of analytical grade and used as received without further purification. Magnetite particles were synthesized as follows: First, argon was bubbled into 100 ml aqueous solution containing 6 mmol (1.20 g) $FeCl_2{\cdot}4H_2O$, 12 mmol (3.25 g) $FeCl_3{\cdot}6H_2O$ and 12 mmol (1.45 g) cysteine for 10 minutes under ultrasonic irradiation. After this deoxidization stage, the solution was rapidly added into 4 M potassium hydroxide at 25 °C while ultrasound irradiation and blowing of argon were still in progress. After 60 minute ultrasonication of the solution under argon atmosphere, a dark suspension was obtained. Centrifuging at 5000 rpm for 10 minutes led to separation of some black precipitates. After washing the products with absolute ethanol and drying at room temperature, the precipitates were dispersed again in 12 mmol cysteine solution for 30 min with ultrasound at 25 °C. This second stage of surfactant addition prevented the particles agglomeration and led to a more stable ferrofluid. In order to study the effect of size distribution on final MR images, three samples were synthesized with various size distributions ensuing from three different elective pH values of the solution; pH = 12 (sample A), pH = 11.5 (sample B) and pH = 11 (sample C) as presented in Table 1. The above-mentioned procedure was repeated three times for each sample and the average results were reported in this work.

Table 1. Experimental conditions for synthesis of samples A, B, C and D.

Sample	A	B	C	D
pH	12	11.5	11	11.5
Second stage of cysteine addition	Yes	Yes	Yes	No
Mean particle size (nm)	9.66	13.22	20.62	13.31
Mean hydrodynamic size (nm)	28.6	41.3	90.0	164.2

In order to investigate the effect of second stage of adding cysteine on the particles' size distribution and particles' agglomeration, some samples were synthesized in the presence of cysteine only at the first stage (sample D). The reaction pH was equal to 11.5 in these experiments.

2.2. Characterizations

X-ray diffraction (XRD) was performed with a Siemens D5000 X-ray diffractometer using graphite-monochromatized high-intensity Cu-K_α radiation (λ = 1.5406 Å). JEOL transmission electron microscope (TEM) JEM-2010F and ZEISS EM-10C one were used to determine the average particle size and morphology of the powders at accelerating voltages of 200 and 80 kV, respectively. Malvern instrument was employed for hydrodynamic diameter measurement via Photon Correlation Spectroscopy (PCS) technique. Samples weight loss with temperature was

evaluated using Thermogravimetric Analysis (TGA) instrument made by PerkinElmer Company.Samples magnetization saturations were measured using Meghnatis Daghigh Kavir Co. Vibrating Sample Magnetometer (VSM).

2.3. Cell culture and cytotoxicity assay

L929 cells were obtained from National Cell Bank of Iran (NCBI), Pasteur Institute of Iran. MTT assay was used to investigate the viability of L929 cells in media containing RPMI1640 (80 % v/v), FBS (10 % v/v) and the ferrofluid sample A (10 % v/v) with various concentrations between 0.224 and 125 μg (Fe)/ml. 0.16 ml of RPMI and 0.02 ml of FBS were distributed in the wells of a 96-well plate. 0.02 ml of the ferrofluid was inserted in each well too. The L929 cells containing solution of RPMI, FBS and magnetite nanoparticles, were cultivated for 24 h in a 5% CO_2 balanced-air incubator at 37 °C. The concentration of cells in each well was fixed to 10^4 cells/ml by counting initial cells with a haemacytometer. In each MTT test, the RPMI-FBS medium was used as control without ferrofluid. After 24 h of incubation, 0.04 ml of MTT solution was added to each well which was followed up by another 4 h of incubation. After removing the medium, 0.05 ml of dimethyl sulfoxide (DMSO) was added to each well to dissolve the formed crystals. Finally, light absorbance was measured at 540 nm by ELISA plate reader. Each MTT test was conducted 3 times with 4 repetitions for each ferrofluid concentration and the average results were reported.

2.4. Magnetic resonance imaging studies

All rats were approved by the "Animal Care and Use Committee" of Tehran Medical University and used through in vivo MRI tests accordingly: Rats were anaesthetized with pentobarbital sodium at the dose of 40 mg/kg body weight and fixed in MRI system. MRI scan was performed 6 h after subcutaneous administration of samples A and B at a dose of 2.5 mg (Fe)/kg body weight. MRI studies were performed at 1.5 T using knee coil for transmission and reception of the signal.

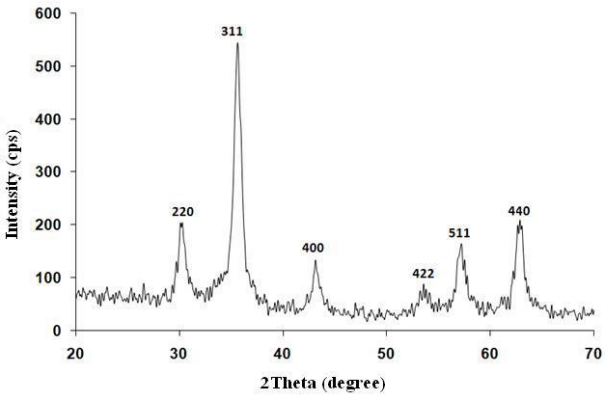

Fig. 2. XRD pattern of sample C.

3. Results and discussion

3.1. X-ray diffraction

XRD pattern of sample C is presented in Fig. 2. Six characteristic peaks for Fe_3O_4 nanoparticles (2θ = 30.16°, 35.48°, 43.13°, 53.49°, 56.91° and 62.71°) marked by their indices (220), (311), (400), (422), (511) and (440) respectively, were recognized for this sample. These peaks are well-matched with the magnetite characteristic peaks (JCPDS card no. 19-0629) confirming the inverse spinel structure of the particles.

3.2. Transmission electron microscopy

TEM images of synthesized nanoparticles with different values of reaction pH are shown in Figs. 3a to 3e. As it can be seen in these figures, the size of nanoparticles is decreased with increasing pH value. The regular distribution of Fe_3O_4 nanoparticles is attributed to the ultrasonic irradiation and the use of cysteine as the biocapping agent in this sample. With the onset of Fe_3O_4 nuclei formation, carboxylic and mercaptan functional groups on the cysteine coordinate to the surface of the Fe_3O_4 nanoparticles leading to the formation of a six-membered chelate ring, as shown in Fig. 4. Consequently, each nucleus would be surrounded by cysteine, which prohibits the excess growth of the nuclei, hence fine nanoparticles are formed. Then, the second stage of adding surfactant in ultrasonicating conditions reduces agglomeration. Measuring 50 particles for each sample, the mean

particle sizes were calculated as 9.66, 13.22 and 20.62 nm for samples A, B and C, respectively (Fig. 5). TEM image of sample C prepared at 80 kV is shown in Fig. 3d. The uniform ring around the particles cannot be seen easily at 200 kV because the high energy electron beam evaporates the surfactant layer at this high voltage. The surfactant layer thickness is about 1.1 nm in Fig. 3d.

The TEM image of sample D, synthesized at pH = 11.5 without second stage of cysteine addition, is shown in Fig. 3e. The mean particle size of sample D was determined as 13.31 nm which is close to that of sample B. By comparing Figs. 3b and 3e, it is clear that particles' agglomeration is more sever in the case of sample D. This fact is well verified with results obtained from hydrodynamic size measurements (Fig. 6).

3.3. Photon correlation spectroscopy

The hydrodynamic size histograms of samples A, B, C and D are illustrated in Figs. 6a, 6b, 6c and 6d, respectively. These data were obtained from PCS measurement. Hydrodynamic size of nanoparticles is decreased as the pH value of the samples is increased. Mean hydrodynamic size of 28.6, 41.3, 90.0 and 164.2 nm was obtained for samples A, B, C and D respectively (Fig. 7). Size distribution in sample A is sharper than that of samples B and C. Decreasing the amount of KOH in the synthesis process leads to the reduction of pH of the reaction solution from 12 to 11, which results in the decrease of particles' surface charge and thus the enlargement of particles' size through an aggregation mechanism. So, mean particle size and mean hydrodynamic size increase with pH decrease. The large amount of mean hydrodynamic size of sample D is due to the single stage process of cysteine addition.

3.4. Thermogravimetric analysis

Fig. 8 shows that the percentage weight loss of sample C due to decomposition of probably organic phase is about 7.4 wt. % above 100 °C. Some simplifying assumptions can be made to calculate the coating density. First, magnetic core is pure magnetite. This assumption is in a good agreement with XRD pattern of the sample (Fig. 2). Thus, the core density can be assumed equal to 5.15 g·cm^{-3}. Second, the magnetic core has a nearly spherical shape. Third, the average coating thickness surrounding all particles is about 1.1 nm. TEM image (Fig. 2b) confirms this assumption. Forth, the mean magnetite core size is about 20.62 nm (TEM Figs. 2a and 2b). Using these assumptions, the coating density is simply calculated to be 1.16 g·cm^{-3}. Comparing with solid L-Cysteine density of 1.67 g·cm^{-3}, this means that a rather high density coating is formed that satisfies the fundamental conditions of formation of a stable ferrofluid. This is in a good agreement with the fact that the synthesized ferrofluids in this work were stable more than 2 months.

3.5. Magnetic measurement

Figs. 9a, 9b and 9c show VSM diagrams of samples A, B and C at room temperature, respectively. Superparamagnetic behavior of samples A and B is due to small particle size, while hysteresis behavior of sample C with H_c ~52 Oe is related to the large particle size and broad size distribution of Fe_3O_4 nanoparticles. According to Fig. 9, saturation magnetization of samples A, B and C is equal to 64.15, 70.75 and 72.70 emu/g, respectively. These values are significantly larger than similar reported data related to long-chain surfactants [13, 14] due to small fraction of non-magnetic surfactant phase in samples A, B and C. This fact is in a good coincidence with the TGA plot of sample C (Fig. 8).

3.6. Cell culture and cytotoxicity assay results

The results of cell culture in the medium containing ferrofluid sample A with 10 decreasing concentrations are presented in Fig. 10 (ANOVA, $p < 0.05$) in comparison with control. According to this Figure, cell viability in all concentrations is more than 90 %. So, the particles biocompatibility is suitable and the samples can be considered for in vivo applications.

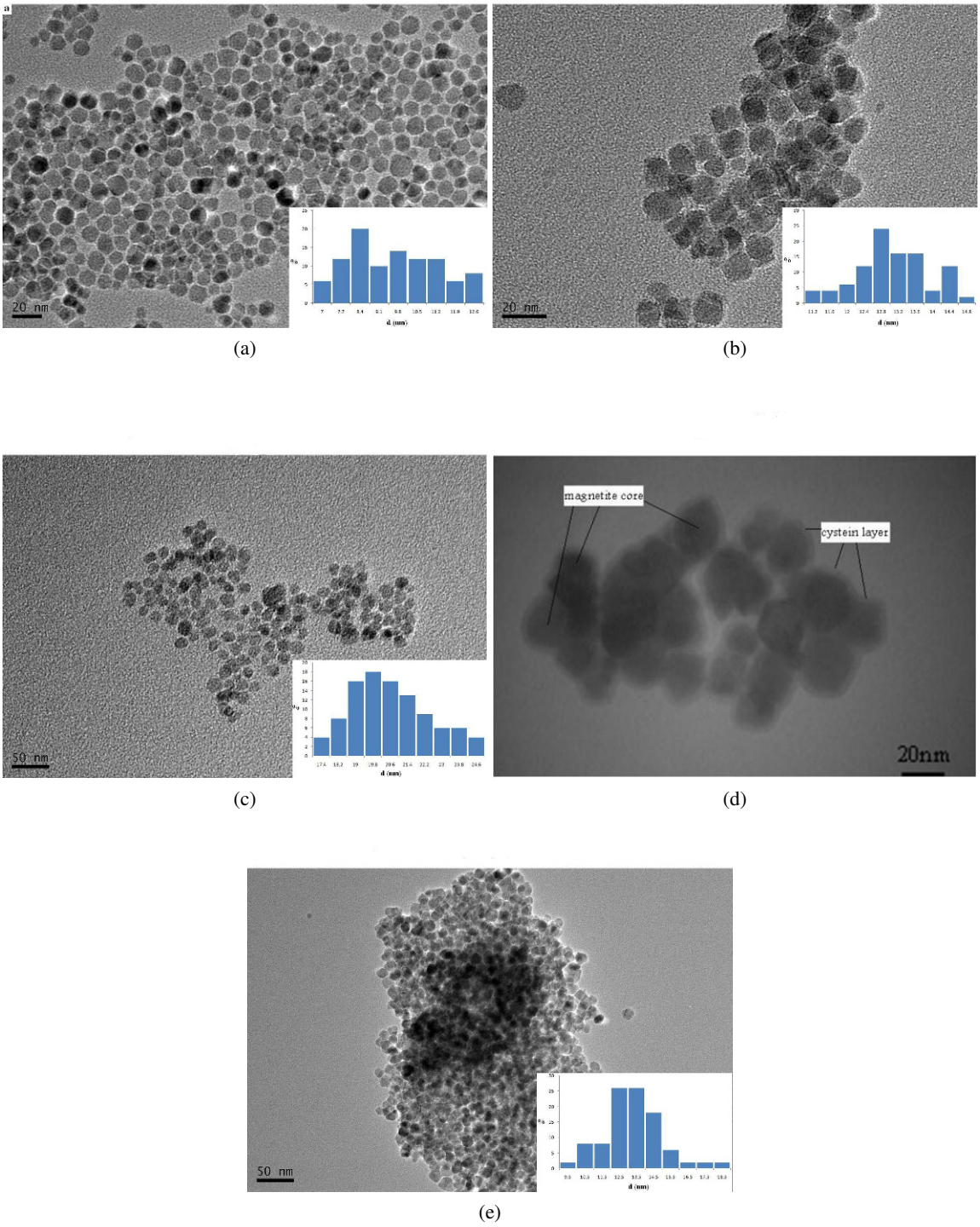

(a) (b)

(c) (d)

(e)

Fig. 3. TEM micrographs of Fe_3O_4 nanoparticles of a) sample A produced at pH = 12 (image prepared at 200 kV), b) sample B produced at pH = 11.5 (image prepared at 200 kV), c) sample C produced at pH = 11 (image prepared at 200 kV), d) sample C (image prepared at 80 kV) and e) sample D produced at pH = 11.5 without second stage of cysteine addition (image prepared at 200 kV).

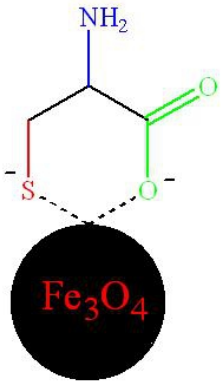

Fig. 4. Proposed structure in the interaction between cysteine and Fe_3O_4 nanoparticle surface.

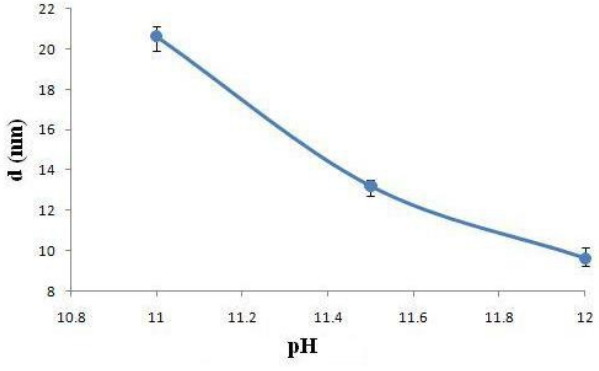

Fig. 5. Diagram showing mean particle size versus pH (n = 3). Each mean size was calculated by measuring 100 particles (Fig. 5).

3.7. Magnetic Resonance Imaging

As it can be seen in MR images of Fig. 11, dramatic decrease of signal intensity in rat lymph nodes confirms the accumulation and susceptibility effect of magnetite nanoparticles. According to these images, 6 hours after subcutaneous injection of sample A and B, lymph nodes were visualized (elliptical marks). As it is explained by theory [21], large and aggregated particles are mainly accumulated in tissues such as liver and spleen, however the smaller ones (20 – 40 nm) are phagocytosed by macrophages of lymphatic system which enhances the image contrast of target tissues through signal intensity decrease in these

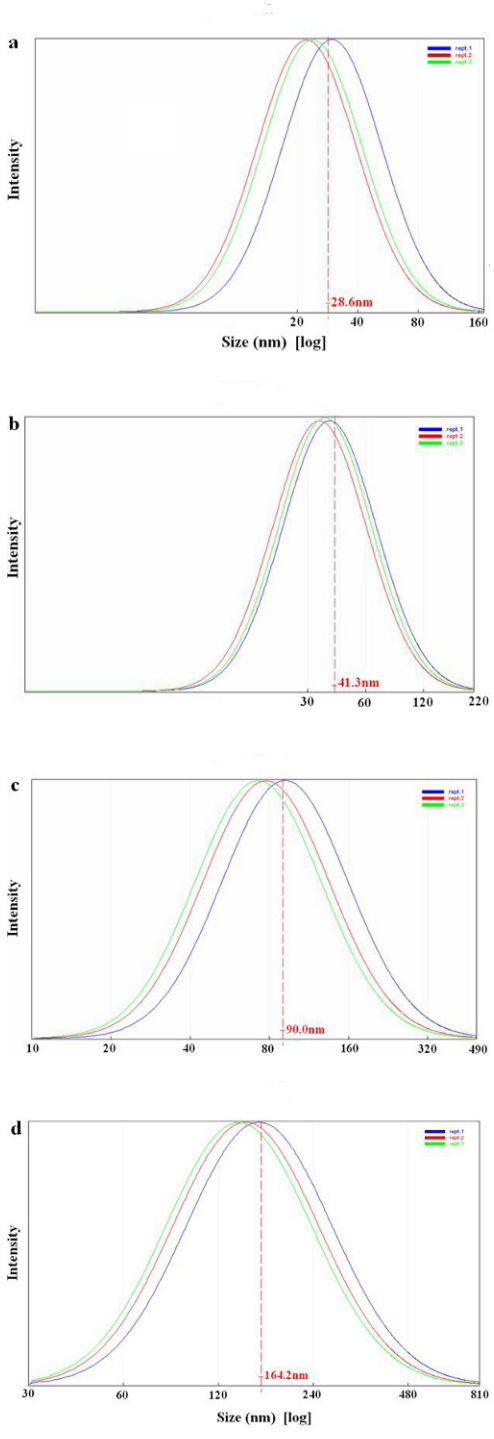

Fig. 6. Size histogram of the samples: a) sample A produced at pH = 12, b) sample B produced at pH = 11.5, c) sample C produced at pH = 11 and d) sample D synthesized at pH = 11.5 without the second stage of surfactant addition. These data were obtained from PCS measurement.

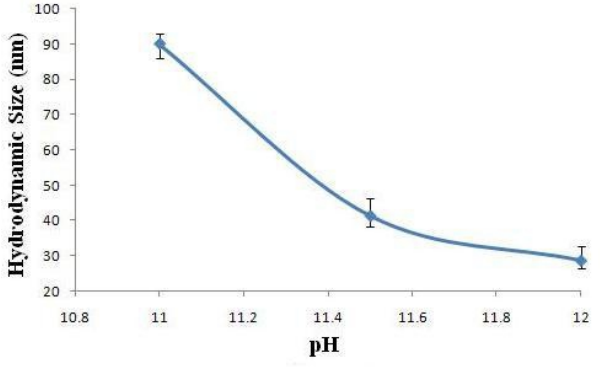

Fig. 7. Diagram showing the mean hydrodynamic size of synthesized samples versus pH (n = 3).

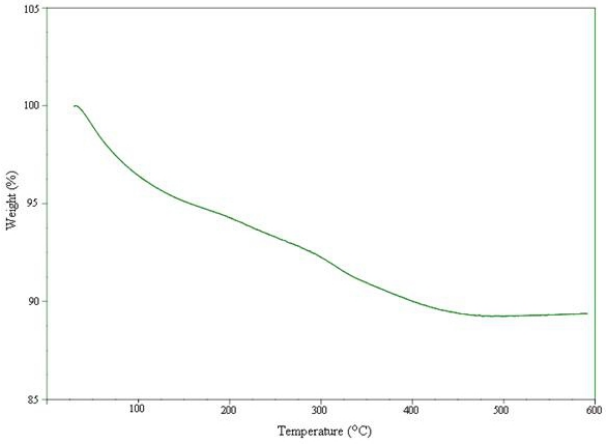

Fig. 8. TGA diagram of sample C.

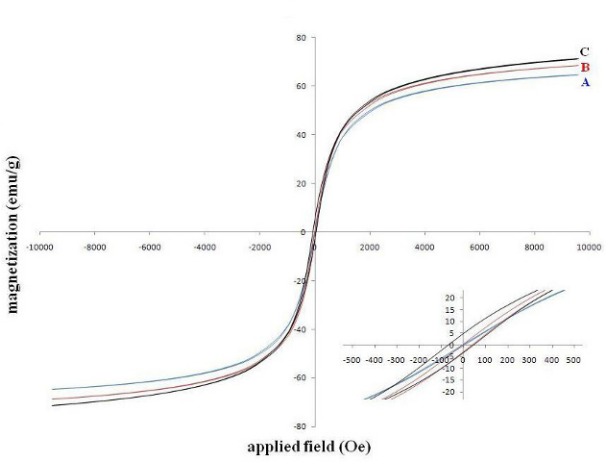

Fig. 9. VSM diagram of a) sample A produced at pH = 12, b) sample B produced at pH = 11.5 and c) sample C produced at pH = 11.

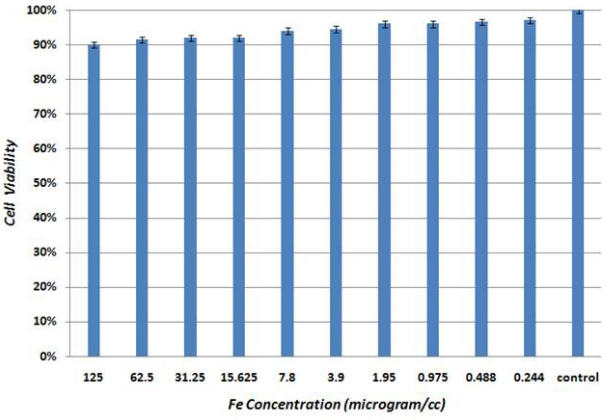

Fig. 10. Viability of L929 cells in various concentrations of cysteine capped magnetite nanoparticles (n = 3, $p < 0.05$). The cells were cultivated with ferrofluid sample A.

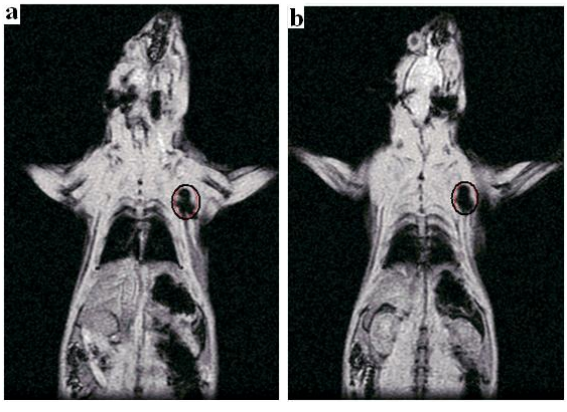

Fig. 11. MR image 6 h after subcutaneous injection of a) sample A and b) sample B at a dose of 2.5 mg (Fe)/kg body weight. Axillary lymph nodes are visualized in these images (elliptical marks).

regions. As subcutaneous injection was done into rats' right hand, no particles' accumulation is seen in the left region of rats' lymph nodes 6 hours after injection. This injection approach was used for easy comparison of two sides, so the regions of particles' accumulation can be recognized easily (elliptical marks in Figs. 11a and 11b).

4. Conclusion

In summary, an ultrasonic-assisted approach for preparation of cysteine-capped Fe_3O_4 nanoparticles was presented. The pH decrease from 12 to 11 led to mean particles size increase from 9.66 to 20.62 nm. Using cysteine as a single-molecule surfactant led to saturation magnetizations of more than 70 emu/g, according to VSM diagrams. An indirect approach was used for the calculation of coating layer density using TGA and TEM results. The coating density, estimated with this approach, was 1.16 g·cm^{-3}. In vitro and animal studies showed that these nanoparticles are well applicable for imaging lymphatic system as contrast agent in MRI.

References

[1] BULTE J. W. M. et al., *Nat. Biotechnol.*, 19 (2001), 1141.

[2] SHAOJUN G., DAN L., LIXUE Z., JING L., ERKANG W., *Biomat.*, 30 (2009), 1881.

[3] FENG B. et al., *J. Alloys Comp.*, 473 (2009), 356.

[4] SEO W. S. et al., *Nat. Mater.*, 5 (2006), 971.

[5] ANG K. L., VENKATRAMAN S., RAMANUJAN R. V., *Mater. Sci. Eng. C*, 27 (2007), 347.

[6] YONGAI Z., FENGQI L., QING Z. GE G., *Coll. Surf. A: Physicochem. Eng. Asp.*, 332 (2009), 98.

[7] AHMADI R., MADAAH HOSSENI H. R., MASOUDI A., *J. Min. Metall. Sect. B-Metall.*, 47 (2011), 211.

[8] XU J. et al., *Magn. Magn. Mater.*, 309 (2007), 307.

[9] WANG C. Y., HONG J. M., CHEN G., ZHANG Y., GU N., *Chin. Chem. Lett.*, 21 (2010), 179.

[10] YUAN Q., VENKATASUBRAMANIAN R., HEIN S., MISRA R. D. K., *Acta Biomat.*, 4 (2008) 1024.

[11] CHEN X., ZHANG Z., QIU Z., SHI C., LI X., *Solid State Commun.*, 140 (2006), 267.

[12] HU C., GAO Z., YANG X., *Mater. Chem. Phys.*, 104 (2007), 429.

[13] ZEFENG X., GUOBIN W., KAIXIONG T., JIANXING L., *J. Magn. Magn. Mater.*, 293 (2005), 182.

[14] KEMPE H., KEMPE M., *Biomat.*, 31 (2010), 9499.

[15] LI B., ZHAO Y., XU X., ZHOU H., HE B., HU Z., ZHANG Z., *Ultrason. Sonochem.* 14 (2007), 557.

[16] KLABER T. L., SMITH C. J., HOWE F. A., *Inves. Radiol.*, 40 (2005), 784.

[17] KIM D. K., ZHANG Y., VOIT W., *Scripta Mater.*, 44 (2001), 1713.

[18] BELLIN M. F., BEIGELMAN C., PRECETTI-MOREL S., *Eur. J. Radiol.*, 34 (2000), 257.

[19] CHO S. J., JARRETT B. R., LOUIE A. Y., KAUZLARICH S. M., *Nanotechnology*, 17 (2006), 640.

[20] LEE J. H. ET AL, *Korean Chem. Soc.*, 28 (2007), 1091.

[21] LACONTE L., NITIN N., BAO G., *Mater. Today*, 8 (2005), 32.

Received 2012-05-02
Accepted 2012-09-04